

Citation for published version:

Zabek, DA, Taylor, J, Ayel, V, Bertin, Y, Romestant, C & Bowen, C 2016, 'A novel pyroelectric generator utilising naturally driven temperature fluctuations from oscillating heat pipes for waste heat recovery and thermal energy harvesting', *Journal of Applied Physics*, vol. 120, no. 2, 024505 (2016), pp. 1-8.
<https://doi.org/10.1063/1.4958338>

DOI:

[10.1063/1.4958338](https://doi.org/10.1063/1.4958338)

Publication date:

2016

Document Version

Peer reviewed version

[Link to publication](#)

This article may be downloaded for personal use only. Any other use requires prior permission of the author and AIP Publishing. The following article appeared in Zabek, D. Taylor, J. Ayel, V. Bertin, Y. Romestant, C. Bowen, C. R. (2016) A novel pyroelectric generator utilising naturally driven temperature fluctuations from oscillating heat pipes for waste heat recovery and thermal energy harvesting. *Journal of Applied Physics*, 120(2) and may be found at <https://doi.org/10.1063/1.4958338>.

University of Bath

Alternative formats

If you require this document in an alternative format, please contact:
openaccess@bath.ac.uk

General rights

Copyright and moral rights for the publications made accessible in the public portal are retained by the authors and/or other copyright owners and it is a condition of accessing publications that users recognise and abide by the legal requirements associated with these rights.

Take down policy

If you believe that this document breaches copyright please contact us providing details, and we will remove access to the work immediately and investigate your claim.

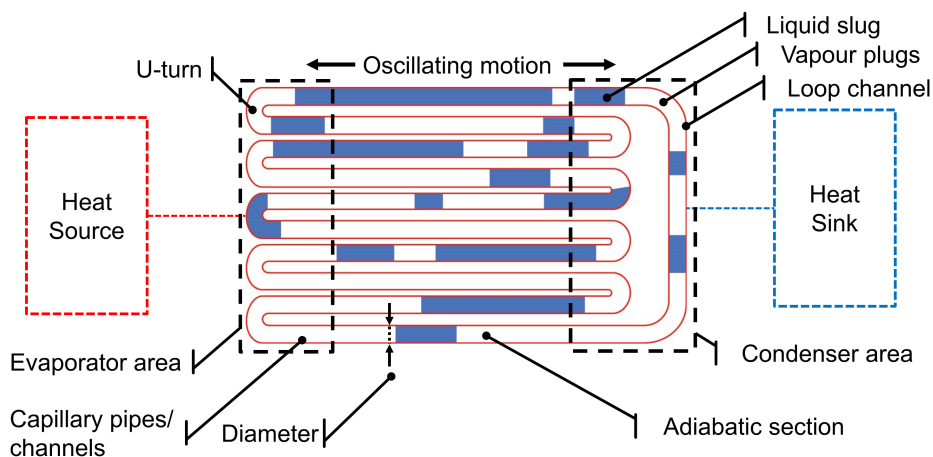
27 1. Introduction

28 The volatile nature of thermal and electrical energy requires a continuous supply with the ability to
29 generate and distribute large scale electric power, since our infrastructure, safety, health and comfort
30 relies on the availability of electricity. Today, over 80 % of the world's electricity is generated from heat
31 [1] and conventional generators such as internal combustion engines (>900 [°C]) or external combustion
32 cycles (>450 [°C]) operate extremely efficiently at such high temperatures. However, the fossil fuel
33 resources, such as coal and gas, which are required to generate high temperatures are limited in
34 availability and the technologies are greatly optimised. At a lower temperature scale, Organic Rankine
35 Cycles (ORCs) are capable of effectively utilising low temperature heat (>150 [°C]), but much of this low
36 grade heat is often not exploited and is simply wasted and released into the atmosphere [2]. This untapped
37 waste heat ranges from thermal management of microprocessors, industrial curing processes, and
38 geothermal sources to more unconventional heat sources such as the human body and contact friction.
39 When exploiting waste heat for energy generation, the generated electricity improves the conversion
40 efficiency of the primary thermal driver and reduces thermal pollution, and is therefore an opportunity for
41 harvesting otherwise unused thermal energy. However, temperatures below 100 [°C] are difficult to
42 recover and to harvest, since the available thermal gradient is low. The use of thermoelectric generators
43 (TEGs) when assembled into a device can be limited, since an effective use of such an approach requires
44 large spatial temperature gradients [3].

45 There is an increasing number of industrial and consumer electronics devices with a need to
46 achieve miniaturisation and circuit integration and this leads to thermally highly concentrated areas which
47 require structurally small heat transfer devices to transport heat. This includes microprocessors, voltage
48 transformers and current rectifiers, since much of the modern electronics requires a direct current (DC),
49 and a wide range of mobile computing devices or electric motors; the use of water-cooling pumps or
50 blower fans is undesirable here due to safety or noise concerns. As a result, the need for more effective
51 heat transfer devices is rapidly growing [4]. The application area of heat pipes and oscillating heat pipes
52 (OHPs), also termed pulsating heat pipes (PHPs), is attracting interest for thermal management or low
53 gradient heat transfer, since they have a high effective thermal conductivity and can be fabricated in
54 almost any shape and size [5]. When an OHP moves thermal energy from one place to another, the
55 naturally driven fluid flow leads to temperature oscillations along the device surface and provides an
56 opportunity for pyroelectric based energy harvesting. Pyroelectric materials produce an electrical current
57 from temperature changes (dT/dt), and can therefore transform the temperature oscillation of an OHPs
58 into electricity while it effectively provides cooling for heat concentrated areas. For such a system, the
59 combination of compact cooling, waste heat recovery and thermal energy harvesting with pyroelectrics is
60 of significant interest since naturally occurring temperature oscillations are often at much lower frequency

61 ($\ll 1\text{Hz}$). Efforts to employ pyroelectric materials for thermal energy harvesting at high frequencies have
 62 led the development of self-induced pyroelectric engines that make use of a bistable membrane for
 63 mechanical switching, generating an open circuit voltage of up to 13 [V] (primarily utilising the
 64 piezoelectric effect since all pyroelectrics are also piezoelectric) [6]. Other theoretical approaches employ
 65 the difference in thermal conductivity between a liquid and a vapour fluid to provide mechanical motion
 66 for a pyroelectric engine [7] or a cantilever structure which mechanically switches the heat flow [8].
 67 However, due to the complexity of these systems the energy trade-off is typically small with
 68 pyroelectrics.

69 In this paper, we propose a novel type of waste heat recovery and thermal energy harvesting
 70 device capable of transforming low temperature fluctuations in oscillating heat pipes into electricity
 71 utilising the pyroelectric effect. The combination of pyroelectrics (P) with oscillating (O) heat (H) pipes
 72 (P) – POHP, enables highly effective heat transfer at low temperatures for transforming heat into
 73 electricity where needed. The proposed POHP system is free of mechanical motion where the pyroelectric
 74 element is powered by the heat that is exchanged within an OHP. This type of generator assembly has the
 75 potential for applications in compact cooling, operation in harsh environments due to the sealed design,
 76 solid-state operation, and utilising a wide range of temperatures by tailoring the working fluid. There is
 77 also potential for miniaturisation of the system with weight reductions and downscaling benefits with
 78 micro fluid systems. In addition, the cooling performance enhancement is expected to be 100 times
 79 greater than conventional cooling systems due to the variable surface tension with fluid mixtures and the
 80 possibility of a supercritical evaporation [9]. The POHP generator can therefore be considered as an
 81 efficient low temperature electric power generator and cooling device.



82
 83 *Figure 1: Schematic diagram of closed-loop oscillating heat pipe (OHP).*

84

85 2. Pyroelectric - Oscillating Heat Pipe (POHP)

86 The complex interaction between the different heat transfer principles of conduction, evaporation and
87 condensation is the driving force of a self-sustaining pulsating fluid flow in an OHP system. The OHP
88 device is initially filled with a working fluid in the liquid-vapour saturation state, and is then placed
89 between a hot reservoir (heat source) and a cold reservoir (heat sink). **Figure 1** shows a schematic of a
90 closed-loop OHP device. In the OHP, a single capillary channel that separates the liquid ‘slugs’ by
91 vapour ‘plugs’ moves the working fluid successively through the hot evaporator area (left side in
92 **Figure 1**) and through the cold condenser area (right side in **Figure 1**) [5]. As a result, the working fluid
93 evaporates at the evaporator zone at the left side of **Figure 1** and condenses at the condenser zone at the
94 right side of **Figure 2** to create local pressure difference. The induced liquid-vapour phase transitions
95 creates a self-driven, rapidly pulsating and circulating fluid flow in the looped capillary channel of the
96 OHP [10]. This sudden change in thermodynamic state of the fluid is determined by the fluid temperature,
97 pressure, gravity and fluid surface tension, where the self-arranged fluid continuously absorbs heat at the
98 hot evaporator zone and ejects it at the cold condenser zone after passing through the central adiabatic
99 section (centre of **Figure 1**) [11]. When considering the energy balance, and considering no heat losses to
100 the surroundings, the amount of absorbed heat at the hot side corresponds to the amount of ejected heat at
101 the cold side. A key variable to design a viable OHP device is the hydraulic capillary channel diameter
102 (maximum diameter of channel) that separates the liquid-vapour plugs and slugs by the surface tension of
103 the fluid. By consider the Bond number Bo , which is the ratio between gravitational and capillary forces
104 acting on an isolated bubble in a vertical capillary tube, the first design approach for an OHP is to
105 determine the critical channel diameter [5]:

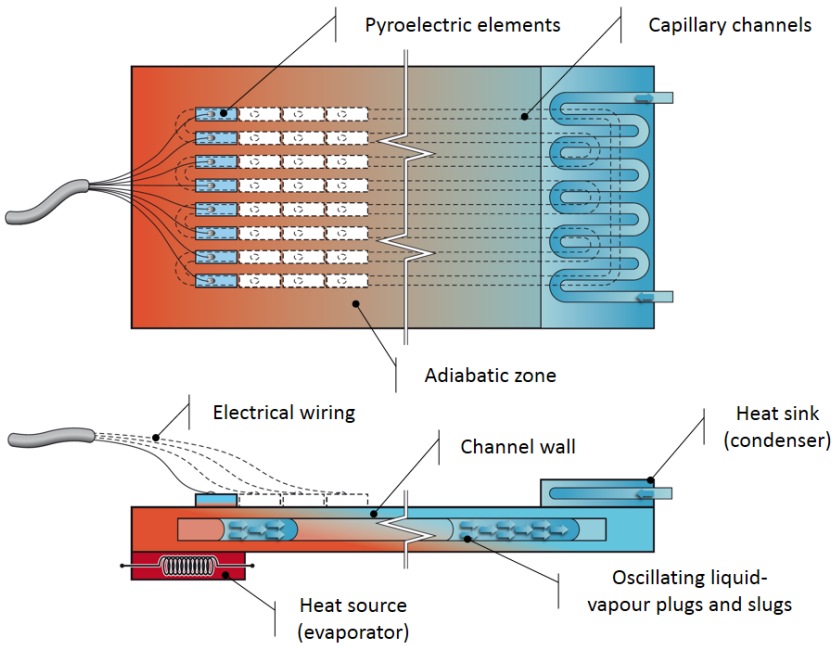
$$106 \quad Bo = \frac{1}{2} \frac{d_h^2 \cdot g (\rho_l - \rho_v)}{\sigma} \quad (1)$$

107 where $\rho_l - \rho_v$ [kg m^{-3}] is the density difference between the two phases (ρ_l = fluid and ρ_v = vapour), and
108 σ [n m^{-1}] is the surface tension of the fluid. The maximum diameter $d_{h,max}$ of the OHP tube is given by:

$$109 \quad \frac{d_{h,max}}{2} \leq \sqrt{\frac{\sigma \cdot Bo}{g (\rho_l - \rho_v)}} \quad (2)$$

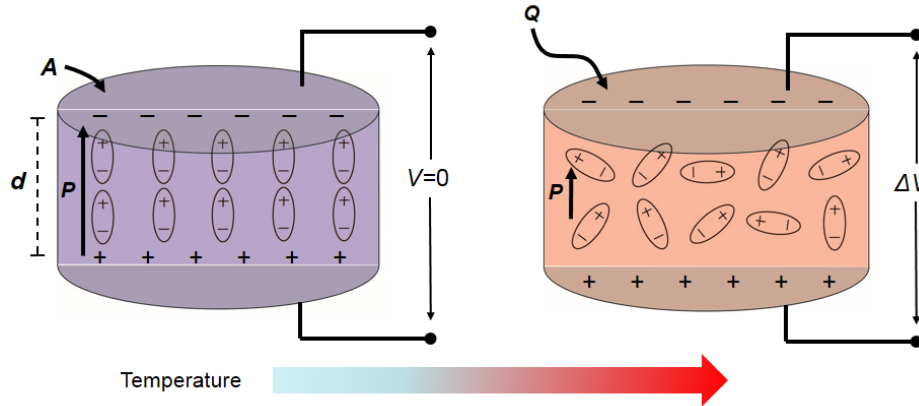
110 **Equation 2** provides a geometrical upper limit of the OHP channel width for maintaining a separation of
111 the slugs and plugs in the tubes. In addition to the channel diameter, other design parameters include the
112 viscous pressure that increases along the channel length and limits fluid motion and is therefore a
113 secondary geometrical limitation. In addition to the channel design, the selection of the working fluid
114 influences the operation of an OHP with surface tension, latent heat, liquid viscosity and the pressure
115 gradients, determining the characteristic liquid-vapour plug and slug separation in **Figure 1**. At the

116 evaporator area, the emergence of evaporation and nucleated bubbles is the driving force of the natural
117 and self-sustaining bubble train flow.



118
119 *Figure 2: Working principle of a POHP generator with the hot evaporator on the left and the cold*
120 *condenser on the right side.*

121 **Figure 2** shows a top- and a cross-sectional view of the capillary channels embedded in an OHP device.
122 As a result of the change in heat transfer properties of the liquid slugs and gaseous plugs phases, they also
123 exchange heat along the adiabatic channel wall of the OHP with local fluctuations in temperature. If we
124 consider a pyroelectric element attached to the channel wall, as shown in the left side of **Figure 2**, the
125 passing slugs and plugs sequentially heat and cool the pyroelectric element respectively. Since a
126 pyroelectric directly converts a change in temperature into an electrical potential difference, the
127 temperature variations induced by the passing liquid slug - vapour plug flow can create an alternating
128 current (AC) proportional to the heat exchange between the fluid and the pyroelectric through the channel
129 wall. While thermoelectric modules based on the Seebeck effect (TEGs) recover heat from spatial
130 temperature gradients, the available transient change in temperature (dT) with OHPs changes the
131 polarisation P [$C\ m^{-2}$] of a pyroelectric material [12].



132

133

Figure 3: Simplified image of pyroelectric energy harvesting.

134 For the pyroelectric elements attached to the OHP channel wall, as in **Figure 2**, **Figure 3** shows the
 135 working principle of pyroelectric material to generate electrical energy from a temperature change. When
 136 the polar crystalline pyroelectric materials is heated due to a flux (Q), the increase in temperature (ΔT)
 137 leads to a reduction in the level of polarisation, P , repelling or attracting surface bound charge. When
 138 electrodes are attached perpendicular to the polarisation direction, P , free charge creates a potential
 139 difference ΔV [V] proportional ΔT [K]. For consecutive heating and cooling cycles at the OHP adiabatic
 140 wall, the passing liquid-vapour slugs and plugs inside the OHP channel continuously thermally excite the
 141 pyroelectric generator which then drives an alternating closed circuit current I [A]. Under short circuit
 142 conditions the current is defined by [13]:

$$143 \quad I_{closed\ circuit} = A \frac{dP}{dT} \frac{dT}{dt} = A \cdot p \frac{dT}{dt} \quad (3)$$

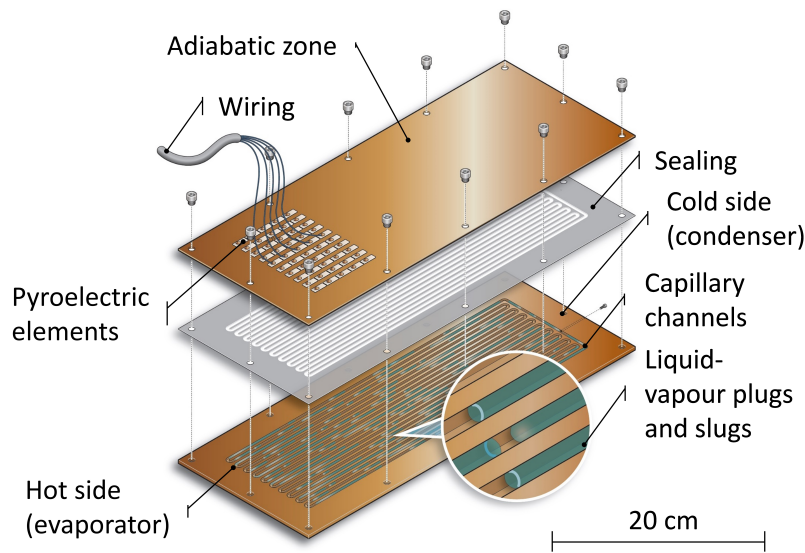
144 and under open circuit conditions the voltage V [V] is given by [14]:

$$145 \quad V_{open\ circuit} = \frac{p}{\epsilon} d \cdot \Delta T \quad (4)$$

146 across the pyroelectric terminals in **Figure 3** and is therefore determined by the materials surface area A
 147 [m^2], pyroelectric coefficient p [$C\ m^{-2}\ K^{-1}$], rate of change in temperature dT/dt [$K\ s^{-1}$], effective
 148 permittivity ϵ [$F\ m^{-1}$], and generator thickness d [m]. When a pyroelectric material (P) is combined with
 149 an oscillating (O) heat (H) pipe (P), POHP, and the assembly operates under a constant heat source and
 150 sink conditions, the POHP moves heat from the hot side to the cold side while continuously thermally
 151 exciting the pyroelectric element divining a AC across the generator terminals. By carefully choosing the
 152 organic working fluids used in the POHP, the phase transition temperature of the evaporation of the
 153 system can be adjusted to the available temperature level to tailoring the cooling performance under
 154 different thermal conditions for compact cooling applications while simultaneously generating electricity
 155 from small temperature differences.

156 **3. Methodology**

157 For low temperature gradients, Akacshi [15] introduced a tubular shaped looped OHP partially filled with
158 a working fluid which acted as a powerful heat transfer and cooling device. Compared to a tubular OHP
159 design, flat plate heat pipes combine a high heat flow and a compact design, which is considered a more
160 efficient approach [16]. Tubes fabricated from copper lead to high heat transport rates with minimal
161 temperature gradients due to the high thermal conductivity of the material [17]. In this work we therefore
162 employed a 20 channel flat plate OHP design (1.6 x 2.0) [mm²] (**equation 1**) and (**equation 2**) with 12 U-
163 turns machined into a 2 [mm] thick copper base plate (30 x 12) [cm²] (**Figure 4**).

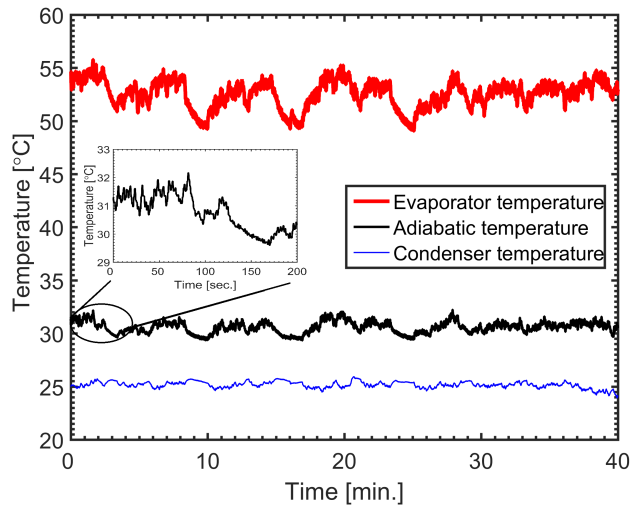


164
165 *Figure 4: OHP with a pyroelectric generator attached to the wall showing a common ground and*
166 *connected to an electrometer using the attached wires for pyroelectric voltage and current measurements*

167 This plate was covered with a second plate with the same dimensions and 1 [mm] of thickness, where the
168 adjacent channels were sealed off relative to one another. The evaporator zone of the flat plate pulsating
169 heat pipe in **Figure 2** and **Figure 4** was heated by a wire electrical heater (Thermocoax Type ZEZA10)
170 that was embedded in a copper plate with dimensions of (10 x 120) [mm²] and 2 [mm] thick by means of
171 a serpentine groove machined on one side of the plate. The heater was connected to electrical power
172 supply (EA ELEKTRO-AUTOMATIK model PS8360-10T). On the opposite side, the condenser zone
173 (80 [mm] long and 120 [mm] wide) was cooled by an ethylene-glycol/water mixture flow that crossed an
174 aluminium block whose temperature was controlled by means of a cryostat (HUBER CC240wl). Good
175 contact between both surfaces (OHP and aluminium condenser) was provided by screws through OHP
176 holes that uniformly distributed the pressure contact. A pressure sensor (GE PTX5076-TA-A3-CA-H0-
177 PS) allowed recording of the pressure levels and fluctuations in the surrounding loop channel. The OHP

178 was filled with ethanol as working fluid with a filling ratio (liquid volume on total channels volume ratio)
 179 of 50 %, where the horizontally orientated channels guide the circulating fluid through the system.

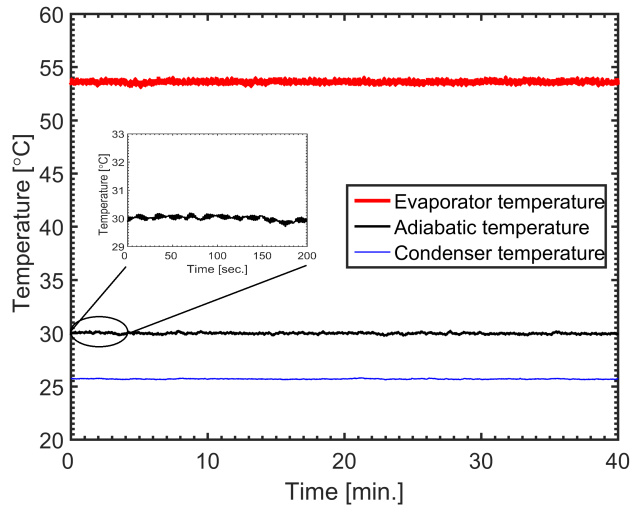
180 **Figure 4** shows the design of our flat plate closed loop Pyroelectric - Oscillating Heat Pipes
 181 (POHP) harvesting and cooling set-up, where the pyroelectric elements are placed directly above the
 182 capillary channels of the OHP, where the pyroelectric is placed to generate electricity. For the liquid-
 183 vapour plugs and slugs, the orientation of the OHP wall is of particular interest since the gravitational
 184 force acting on the bubbles leads to a continuous aggregation of liquid at the evaporator zone, particularly
 185 in vertical orientation (bottom heated mode). Therefore, we examine two positions, one with the gravity
 186 acting planar to the OHP wall (vertical position), and the other with the gravity acting in a 45° angle
 187 perpendicular to the wall. In both positions the boundary conditions are maintained constant with the
 188 resistive electric heating power fixed at 120 [W] and the chiller, maintaining the cold condenser
 189 temperature at 20 [°C]. The experiments were conducted over several hours in order to establish constant
 190 average temperatures. If the device to be cooled acts as a heat source (left side **Figure 2** and **Figure 4**),
 191 the spatial temperature gradient across the system introduces liquid plugs and vapour slugs which
 192 exchange heat along the channel wall of the OHP leading to fluctuations in temperature at a relatively
 193 high frequency; we will see later in the paper that typical frequencies and temperature changes are 0.45
 194 Hz and 5 [K] respectively.



195
 196 *Figure 5: OHP temperature map for 45° operation at an arbitrary chosen time window.*

197 **Figure 5** shows the local temperature profile measured at the evaporator (highest temperature), the
 198 adiabatic zone and the condenser (lowest temperature) for the 45° tilted wall of the OHP. The
 199 temperatures were measured using K-type thermocouples located across the OHP wall. Although the
 200 system was synchronised between the evaporator and the condenser, thereby showing an identical

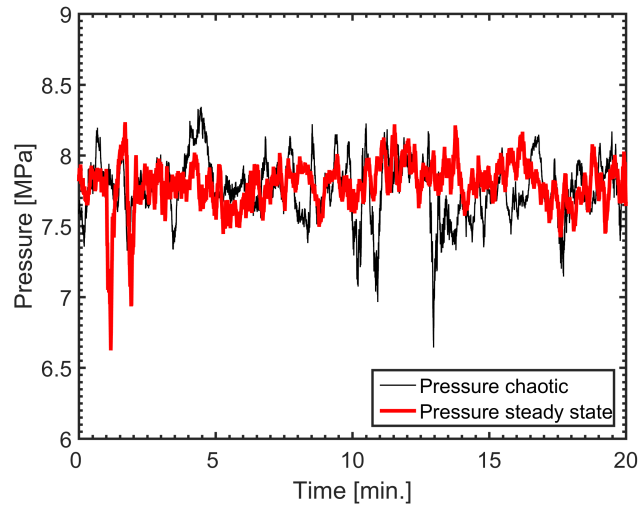
201 temperature envelope, the fluid flow is chaotic and leads to random changes in temperature (dT), starting
 202 from 0.1 [K] at the condenser to 5 [K] at the evaporator with no particular temperature oscillation
 203 frequency. A Fast Fourier Transformation (FFT) analysis did not reveal any characteristic or natural
 204 frequency providing a constant line across the frequency spectrum. Therefore, there is no evidence for
 205 distinctive temperature oscillation frequencies. This leads to the conclusion that the transient temperature
 206 profile is highly unsteady due to the two-phase instability of the working fluid under certain thermal and
 207 geometrical boundary conditions [18].



208
 209 *Figure 6: OHP temperature map for 0° operation at an arbitrary chosen time window.*

210 With horizontally orientated channels (planar gravity), **Figure 6** shows the temperatures across all three
 211 OHP zones (evaporator, adiabatic and condenser). With an average evaporator temperature of 54 [°C], a
 212 chiller temperature of 26 [°C], and a temperature gradient of 28 [°C], the OHP operates at a steady state
 213 oscillation frequency of 0.45 [Hz]. Continuous and symmetric temperature oscillations are observed along
 214 the adiabatic zone with a temperature oscillation magnitude of 0.3 [K]; e.g. see the inset in **Figure 6**. The
 215 temperature oscillations at the OHP wall that are shown in **Figure 5** and **Figure 6** stem from the heat,
 216 exchanged with the surrounding environment, which can be utilised to successively heat and cool a
 217 pyroelectric generator attached to the wall surface. In order to achieve rapid (**Equation 3**) and large
 218 (**Equation 4**) temperature oscillations to maximise the pyroelectric signal we found from thermocouple
 219 measurements that the highest oscillation magnitude takes place at the lower region of the adiabatic zone,
 220 which is closer to the hot evaporator. At steady state operation conditions, as in **Figure 6**, the temperature
 221 constantly fluctuates between 38.4 [°C] and 39.7 [°C] leading to an available change in temperature of
 222 0.3 [K] at 0.45 [Hz]. Compared to already existing pyroelectric thermal harvesters operating in the lower
 223 mHz oscillation range [19], the temperature oscillations frequencies in a POHP system are therefore much

224 larger and faster.



225

226 *Figure 7: Condenser pressure for chaotic and steady state operation of the OHP at the loop channel.*

227 Since the available thermal gradients are low at the condenser section, the corresponding liquid-vapour
228 pressure difference is also low. When a pressure sensor was placed at the surrounding looped channel of
229 the cold condenser zone to measure the transient pressure, **Figure 7** shows the pressure fluctuations for
230 both chaotic and steady state OHP operation. Since the fluid flow at low temperature and pressured
231 gradients is perpendicular to the rest of the channel, pressure for chaotic operation and steady state
232 operation are indistinguishable. However, as shown in **Figure 5** and **Figure 6**, the OHPs provide large
233 and rapid naturally driven temperature oscillations without mechanical switching which are ideally suited
234 to power a pyroelectric generator attached to the wall surface.

235 **4. Results and discussion**

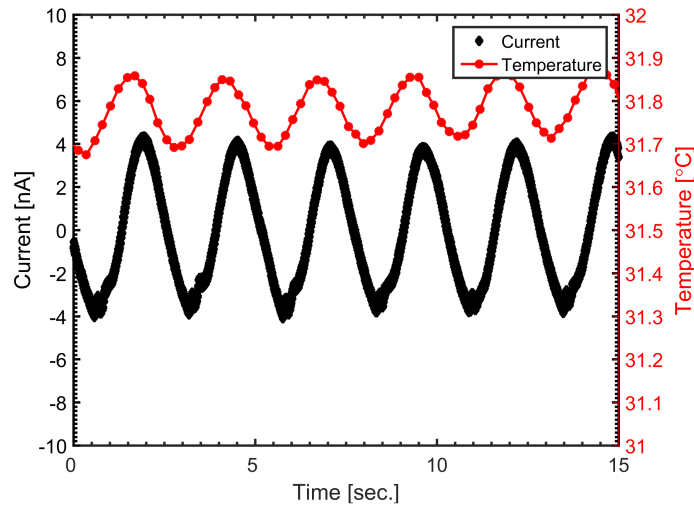
236 Compared to flexible polyvinylidene difluoride (PVDF) pyroelectric active polymers [20], bulk ceramics
237 pyroelectric materials are typically high stiffness and brittle (low fracture toughness) but exhibit
238 significantly higher pyroelectric coefficients. Since pyroelectrics are typically electrically and thermally
239 insulating, the heat exchanged between the OHP and the pyroelectric generator is assumed to be via
240 conduction only, where the contact area between the pyroelectric element and the OHP wall determines
241 the heat flow. In this work we have placed both, a (11 x 3) [mm²] and 500 [μm] thick lead magnesium
242 niobate – lead titanate (PMN-PT) single crystal and a polycrystalline lead zirconate titanate (PZT)
243 (11 x 3) [mm²] and 500 [μm], on the OHP wall directly above the adiabatic channel. Details of the two
244 materials are provided in **Table 1**. **Figure 4** shows the geometrical position and the electrical setup where
245 the pyroelectric was placed 35 [mm] from the heater (evaporator) and 9 [mm] from the edge. The open
246 circuit voltage and the closed circuit current per element was measured using a Keithley 6517b

247 electrometer (input impedance 200 TΩ) at a sampling rate of 100 [Hz] together with the temperature
 248 measurements using a Picotech TC-08 at a sampling rate of 10 [Hz]. A good interface contact between the
 249 pyroelectric element and the OHP wall was ensured using a copper paste (Electrolube-UK) providing a
 250 good thermal and electrical contact with the common ground. A ‘doctor blade’ deposition technique of
 251 the copper paste ensured good homogeneity and repeatability of this process, which is also used in
 252 ISO8301 for measuring conductivity of thermal insulators (e.g. ceramics and polymers). Temperature
 253 measurements were conducted using a leaf K-type thermocouple (OMEGA-US) directly below the
 254 pyroelectric element and encapsulated in the copper paste.

255 *Table 1: Material properties for PMN-PT and PZT.*

	PMN-PT	PZT	Reference
p [$\mu\text{C m}^{-2} \text{K}^{-1}$]	-746	-380	[15]
A [mm^2]	(11 x 3)	(11 x 3)	[-]
d [μm]	500	500	[-]
ϵ [-]	2100	2900	[15]
C [nF]	1.22	0.17	[-]
k [$\text{W m}^{-1} \text{K}^{-1}$]	2	0.8	[15]
T_{Curie} [$^{\circ}\text{C}$]	121	200	[15]
$-p/\epsilon$ [$\mu\text{C m}^{-2} \text{K}^{-1}$]	0.35	0.13	

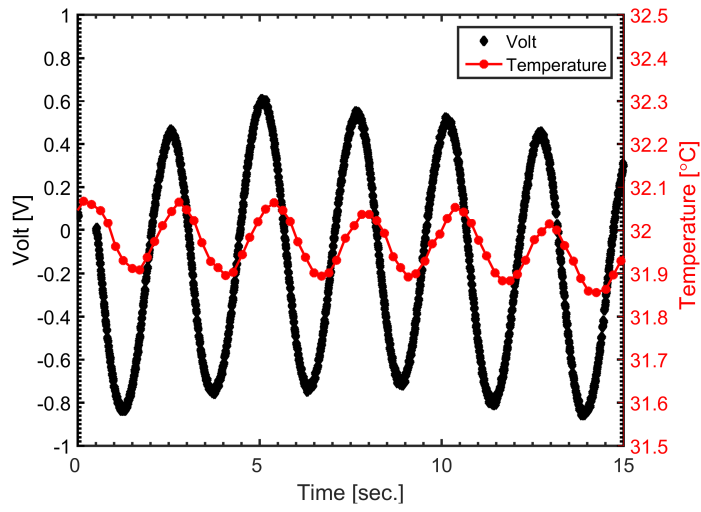
256



257

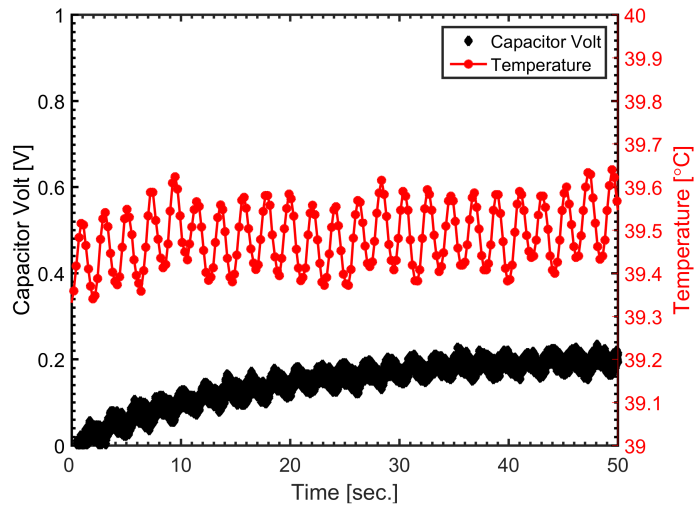
258

(a)



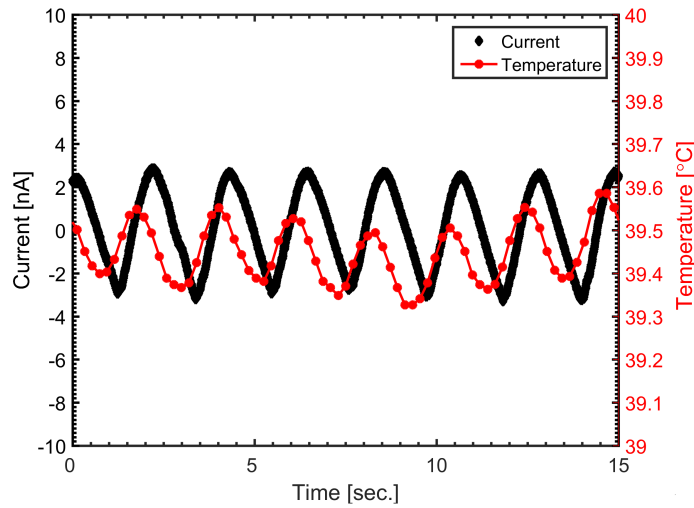
259
260

(b)



261
262

(c)

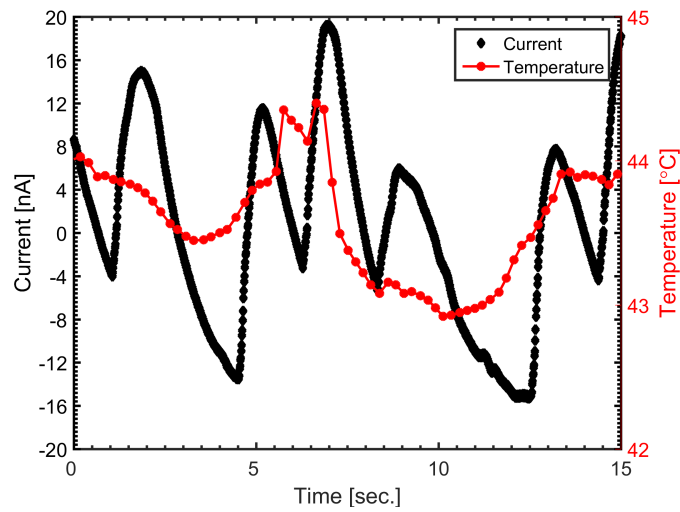


(d)

Figure 8: Closed circuit pyroelectric current with PMN-PT (a), open circuit pyroelectric voltage with PMN-PT (b), capacitor voltage with PMN-PT (c) and closed circuit pyroelectric current with PZT (d) for steady-state OHP operation.

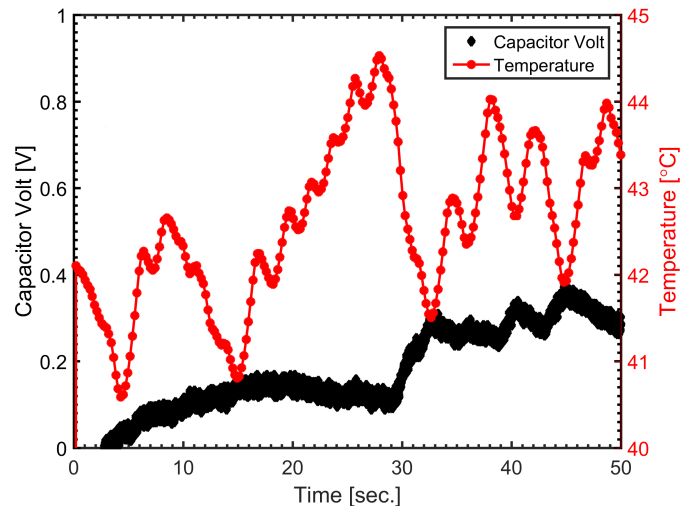
For the steady state operating OHP (Figure 6), Figure 8a compares the recorded symmetric temperature oscillations with a measured pyroelectric closed circuit current of 4.2 [nA], generated by the PMN-PT pyroelectric element. The measured open circuit voltage with PMN-PT was 0.8 [VAC] (Figure 8b). With an available electrical capacitance of 1.22 [nF] for the pyroelectric generator, the transformed electrical energy per thermal evolution stored in the capacitive element ($\frac{1}{2}CV^2$) was 1.56 [nJ cycle⁻¹], which corresponds to a specific energy density of 95 [pJ cm⁻³]. When the generated alternating current (AC) was continuously discharged across a full wave bridge rectifier into a 50 [pF] external capacitor, the available temperature oscillations can charge the external capacitor within 40 sec. to 0.2 [V] (Figure 8c). This rectification stage is required, since the voltage supplied by the generator is an AC, and most of the modern electronics require a direct current (DC). Since electrical energy stored in a capacitive element suffers increasing leakage with increasing voltage, the voltage at the capacitor saturates because the supplied charge from pyroelectric equals the leakage at the external capacitor; suitable selection of low leakage capacitors can improve this response. The single crystal PMN-PT used in this study has been selected as it has an outstanding pyroelectric properties but does exhibit a relatively low Curie temperature (121 [°C]), limiting the potentially usable temperature range. Therefore, measurements have been taken with a polycrystalline PZT material, which can operate at higher temperatures due to the higher Curie temperature of 200 [°C] and consequently can operate at higher temperature levels. However, the pyroelectric coefficient of PZT is lower than PMN-PT (see Table 1) which results in lower

286 closed circuit current measurements under identical operation conditions compared to PMN-PT; the PZT
 287 has a pyroelectric current of 3 [nA] (**Figure 8d**). The corresponding open circuit voltage with PZT was
 288 also lower, 0.4 [V] compared to 0.8 [V] for PMN-PT and relates to the lower p/ϵ ratio of PZT; see
 289 Equation 4 and Table 1. The measured current for PMN-PT and PZT is in reasonable agreement with
 290 the calculated values for current from **Equation 3** (PMN-PT = 3.3 [nA] and PZT = 1.7 [nA]). The
 291 continuous pyroelectric signals together with the harmonic temperature oscillations at the OHP wall lead
 292 to the conclusion that the system operates at steady state with the fluid-vapour bubbles oscillating
 293 symmetrically across the adiabatic zone.



294
 295

(a)



296
 297

(b)

298 *Figure 9: Closed circuit pyroelectric current with PMN-PT (a), and capacitor voltage with PMN-PT (b)*
299 *for unsteady OHP operation.*

300 To achieve chaotic changes in temperature, as in **Figure 5**, the OHP was tilted by 45° with respect to
301 gravity, and the pyroelectric generator was placed in the same position as in steady state operation. **Figure**
302 **9a** shows the generated closed circuit current for a PMN-PT single crystal along with the temperature
303 oscillations at the OHP wall. With a peak current of 20 [nA] the closed circuit current and the change in
304 temperature are significantly higher than in the steady state operation of the OHP (typically 4 [nA],
305 **Figure 8a**). However, no continuous pyroelectric signal can be generated since the temperature
306 fluctuations are unsteady and do not follow a particular pattern. Therefore, a direct discharge of the
307 generated electrical energy across the full wave bridge rectifier into the external 100 [nF] capacitor leads
308 to a capacitor voltage of 0.4 [V] at the capacitor terminals. **Figure 9b** shows the charging profile of the
309 capacitor powered by the pyroelectric PMN-PT with a four times higher rectified and stored energy for
310 unsteady operation of 8 [nJ], compared to 2 [nJ] for steady operation. The temperature fluctuations
311 performed, in both steady and unsteady modes of operation, are highly suitable for pyroelectric thermal to
312 electrical energy conversion, due to the high oscillation frequency of up to 0.45 Hz, providing a new type
313 of thermal to electrical generator operating at low temperatures. Performance enhancements can be
314 achieved by using micro heat pipes of a similar size employed in this work and filled with water-heptanol
315 mixtures that exhibit higher temperature oscillations and larger heat flows [21]. The system conversion
316 efficiency in this work with the POHP and rectification circuit and only one pyroelectric element attached
317 is $\eta = 3.3 \times 10^{-13}$ for the unsteady operation and $\eta = 1.33 \times 10^{-12}$ for the steady operation over 50 sec.,
318 determined by the generated energy (8 [nJ] and 2 [nJ]) over the heater power input (120 [W]). This is
319 lower than the theoretical Carnot efficiency of $\eta_{Carnot} = 0.09 \%$ (55 °C and 25 °C), which leads to the
320 conclusion that there is substantial space for optimisation of the OHP-pyroelectric generator system.
321 Compared to conventional thermo-electric generators (TEGs) operating at an efficiency below 10 %, the
322 here proposed POHP design converts only 0.04 % of the available surface of the OHP with a pyroelectric
323 material providing additional space for improvement by improving the contact area. In addition, two
324 distinctive modes of operation are presented, based on a constant heat input – available electrical output
325 comparison, showing a four times higher energy generation in chaotic mode than in steady state mode.
326 Limitations in transformed energy mainly stem from the poor contact conduction when using structurally
327 thick copper walls which leads to a decrease and a delay in heat flow. It is worth noting that temperature
328 oscillations of a greater amplitude have been observed in the OHP literature [18], suggesting that much
329 larger energy recovery is expected from such systems. For constant temperature oscillations, one
330 approach to improve performance is to introduce grooves into the OHP wall directly above the channel of

331 the working fluid. The generator will ideally to be of equivalent dimensions to the vapour plug
332 displacement inside the channel the fully exploit the temperature fluctuations. For chaotic temperature
333 oscillations, the frequency and magnitude of the oscillations should be enhanced and a more thermally
334 conductive generator geometry with a larger area and patterned electrodes will improve the interface
335 contact conduction.

336 On an industrial scale, integrated cooling and heat recovery units have the potential to utilise the
337 abundantly available heat through an OHP in order to drive a pyroelectric generator and effectively cool
338 heat-concentrated areas without mechanical motion, while also generating electricity locally from the
339 otherwise wasted heat. In the longer term, POHP type of systems can act as solid-state generators and
340 thermal harvesters operating low-carbon micro-grids where the risk of mechanical wear and failure is
341 eliminated. Therefore, POHP systems combine highly desirable solid-state electricity generation with a
342 powerful closed packed cooling device absorbing otherwise unused heat. The thermal performance
343 conversion of the system has the potential to cover range from Watts to kWatts of heat flow, capable of
344 eg. replacing conventional blower fans and large sized heat sinks and providing μ Watts to mW of
345 electrical power, e.g. for wireless sensor nodes, internet of things (IoT) devices or battery-less
346 technologies [22].

347 5. Conclusions

348 This paper presents the recovery of heat using pulsating heat pipes (OHPs) in conjunction with
349 pyroelectric elements provides as a new approach for transforming thermal energy at low temperatures
350 directly into electrical energy, available for discharge. In this paper we are the first to demonstrate that it
351 is possible to exploit the rapid temperature oscillations of an OHP operating in both, steady state and
352 unsteady modes, using a pyroelectric generator to effectively charge a storage capacitor and generate
353 electrical energy while providing cooling. Since no external power supply is required to move the fluid in
354 this solid state assembly, the self-sustaining system and the generated energy provides an additional and
355 alternative power supply for the constantly growing number of electric and electronic devices. This new
356 type of thermal generator uses lead magnesium niobate – lead titanate (PMN-PT) with a flat plate OHP
357 and continuously generates an energy of $95 \text{ [pJ cm}^{-3}\text{]}$ at 0.45 [Hz] without mechanical motion. In the
358 chaotic mode of operation, the system effectively provides four times more electrical energy than in the
359 steady state mode. With potential to further optimise the transformation performance, pyroelectric-
360 oscillating heat pipe (POHP) generators provide a route to cool thermally concentrated areas while also
361 provide electricity that is needed for monitoring and communication tasks or where wireless
362 communication and self-sustaining applications operate remotely. Other potential applications beyond
363 compact cooling are standalone small-scale generators where the unexplored properties of liquid-vapour

364 hysteresis will lead to a more efficient thermal cycling fluid. Due to the nature of the fluid flow, this is a
365 solid-state, 'fit and forget' design with no moving mechanical parts and no need of maintenance while
366 transforming abundantly available waste heat into electrical power.

367 6. References

- 368 [1] Federal Energy Administration (2015) Available: www.energy.gov [Accessed: 30. April 2016].
- 369 [2] Zabek, D., Penton, J. and Reay, D., 2013. Optimization of waste heat utilization in oil field
370 development employing a transcritical Organic Rankine Cycle (ORC) for electricity
371 generation. *Applied Thermal Engineering*, 59(1), pp.363-369.
- 372 [3] Dresselhaus, M.S., Chen, G., Tang, M.Y., Yang, R.G., Lee, H., Wang, D.Z., Ren, Z.F., Fleurial,
373 J.P. and Gogna, P., 2007. New Directions for Low-Dimensional Thermoelectric
374 Materials. *Advanced Materials*, 19(8), pp.1043-1053.
- 375 [4] Fujitsu (2015) Fujitsu Develops Thin Cooling Devices for Compact Electronics. Available:
376 www.fujitsu.com [Accessed: 30. April 2016].
- 377 [5] Ma, H., 2015. *Oscillating heat pipes*. Springer.
- 378 [6] Ravindran, S.K.T., Huesgen, T., Kroener, M. and Woias, P., 2011. A self-sustaining micro
379 thermomechanic-pyroelectric generator. *Applied Physics Letters*, 99(10), p.104102.
- 380 [7] Cha, G. and Ju, Y.S., 2013. Pyroelectric energy harvesting using liquid-based switchable thermal
381 interfaces. *Sensors and Actuators A: Physical*, 189, pp.100-107.
- 382 [8] Mostafa, S., Lavrik, N., Bannuru, T., Rajic, S., Islam, S.K., Datskos, P.G. and Hunter, S.R., 2011.
383 A Finite Element Model of Self-Resonating Bimorph Microcantilever for Fast Temperature
384 Cycling in A Pyroelectric Energy Harvester. In *MRS Proceedings* (Vol. 1325, pp. mrrs11-1325).
385 Cambridge University Press.
- 386 [9] Mochizuki, M., Saito, Y., Kiyooka, F., Nguyen, T., Nguyen, T. and Wuttijumnong, V., 2007,
387 January. Advanced micro-channel vapor chamber for cooling high power processors. In *ASME*
388 *2007 InterPACK Conference collocated with the ASME/JSME 2007 Thermal Engineering Heat*
389 *Transfer Summer Conference* (pp. 695-702). American Society of Mechanical Engineers.
- 390 [10] Lips, S., Bensalem, A., Bertin, Y., Ayel, V., Romestant, C. and Bonjour, J., 2010. Experimental
391 evidences of distinct heat transfer regimes in pulsating heat pipes (PHP). *Applied Thermal*
392 *Engineering*, 30(8), pp.900-907.
- 393 [11] Tong, B.Y., Wong, T.N. and Ooi, K.T., 2001. Closed-loop pulsating heat pipe. *Applied thermal*
394 *engineering*, 21(18), pp.1845-1862.
- 395 [12] Sebald, G., Guyomar, D. and Agbossou, A., 2009. On thermoelectric and pyroelectric energy
396 harvesting. *Smart Materials and Structures*, 18(12), p.125006.
- 397 [13] Lang, S.B., 2005. Pyroelectricity: from ancient curiosity to modern imaging tool. *Physics*
398 *Today*, 58(8), pp.31-36.

- 399 [14] Bowen, C.R., Taylor, J., LeBoulbar, E., Zabek, D., Chauhan, A. and Vaish, R., 2014. Pyroelectric
400 materials and devices for energy harvesting applications. *Energy & Environmental*
401 *Science*, 7(12), pp.3836-3856.
- 402 [15] Akachi, H., Actronics Kabushiki Kaisha, 1990. *Structure of a heat pipe*. U.S. Patent 4,921,041.
- 403 [16] Reay, D., McGlen, R. and Kew, P., 2013. *Heat pipes: theory, design and applications*.
404 Butterworth-Heinemann.
- 405 [17] Ayel, V., Araneo, L., Scalambra, A., Mameli, M., Romestant, C., Piteau, A., Marengo, M.,
406 Filippeschi, S. and Bertin, Y., 2015. Experimental study of a closed loop flat plate pulsating heat
407 pipe under a varying gravity force. *International Journal of Thermal Sciences*, 96, pp.23-34.
- 408 [18] Górski, G., Litak, G., Mosdorf, R. and Rysak, A., 2015. Two phase flow bifurcation due to
409 turbulence: transition from slugs to bubbles. *The European Physical Journal B*, 88(9), pp.1-6.
- 410 [19] Zhang, Q., Agbossou, A., Feng, Z. and Cosnier, M., 2011. Solar micro-energy harvesting with
411 pyroelectric effect and wind flow. *Sensors and Actuators A: Physical*, 168(2), pp.335-342.
- 412 [20] Zabek, D., Taylor, J., Le Boulbar, E., and Bowen, CR.; "Micropatterning of Flexible and Free
413 Standing Polyvinylidene Difluoride (PVDF) Films for Enhanced Pyroelectric Energy
414 Transformation." *Advanced Energy Materials* 5, no. 8 (2015).
- 415 [21] Hu, Y., Liu, T., Li, X. and Wang, S., 2014. Heat transfer enhancement of micro oscillating heat
416 pipes with self-rewetting fluid. *International Journal of Heat and Mass Transfer*, 70, pp.496-503.
- 417 [22] Somov and Giaffreda (2015) Powering IoT Devices. Technologies and Opportunities. Available:
418 iot.ieee.org [Accessed: 30. April 2016].

419 7. Acknowledgements

420 The research leading to these results has received funding from the European Research Council under the
421 European Union's Seventh Framework Programme (FP/2007-2013) / ERC Grant Agreement no. 320963
422 on Novel Energy Materials, Engineering Science and Integrated Systems.